

Fundamental study of surface densification of PM gears by rolling using FE analysis

Fritz Klocke · Tobias Schröder · Philipp Kauffmann

Received: 16 February 2007 / Accepted: 9 March 2007 / Published online: 8 August 2007
© German Academic Society for Production Engineering (WGP) 2007

Abstract The complex shape of gears is very attractive to the near-net-shape PM technology. The strength of conventional PM parts is reduced by the residual porosity due to the power law relationship between the density and the mechanical properties. The maximum stresses in gears are found in the tooth root and the flank near or directly at the surface, so that by a local densification of the near surface layer the maximum load carrying capacity of the complete gear can be increased. This surface densification can be achieved by a rolling process. Due to the own elastic-plastic behavior of PM materials and due to the continuous change of the contact conditions during rolling, the process is too complex to be described analytically. To gain a better understanding of the process, the numerical simulation is a capable method. In this paper an FEA model is prepared and verified based on an experimental investigation. Additionally, case studies were carried out in order to analyze the relationship between the process parameters and the densification result.

Keywords Production process · Powder metallurgy · Numerical simulation

1 Introduction

Driven by globalization the industry is facing an increasing competition. Therefore it becomes more and more neces-

sary to consider alternative technologies such as powder metallurgy in order to exploit cost saving potentials.

The high-volume production industry such as the automobile industry has already recognized the advantages of the near net shape manufacturing process powder metallurgy including little finishing operations, optimal utilization of raw material, short cycle times and favorable energy consumption. Compared to conventional manufacturing technologies, the powder metallurgy has experienced a worldwide growth in the last decades, due to innovations in the fields of namely the optimization of the compaction cycle, optimized sintering conditions, density increase and optimized heat treatment conditions. Most of the structural part applications are placed in passenger cars, e.g. ABS rings, oil pump pinions, camshafts, chain sprockets or synchronizer hubs. Nowadays, the typical US passenger car contains more than 20 kg of sintered parts, a figure that will increase within the next several years.

2 Influence of the density on mechanical properties

The porosity of sintered parts causes an internal notch effect. Thus the properties of sintered parts depend on the density of the material. According to Beiss [1], most properties can be described by a parabolic function based on the relative density, see equation 1.

$$\frac{P}{P_0} = \left(\frac{\rho}{\rho_0} \right)^m = \rho_{rel} \quad (1)$$

P : property, P_0 : property in full dense state
 ρ : density, ρ_0 : density of the pore-free state
 m : property and pore morphology dependent constant

The investigations described in this present paper were sponsored by the WZL Gear Research-Circle.

F. Klocke · T. Schröder · P. Kauffmann (✉)
Laboratory of Machine Tools and Production Engineering,
RWTH Aachen University, Aachen, Germany
e-mail: p.kauffmann@wzl.rwth-aachen.de

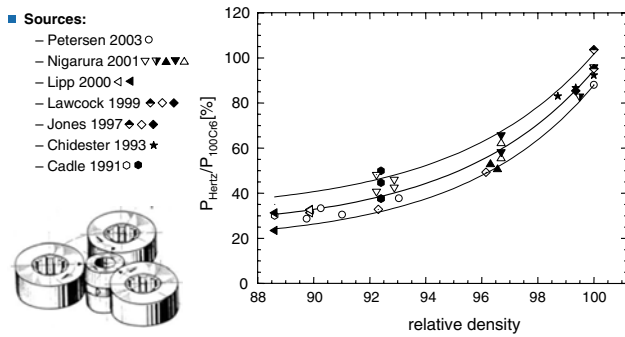


Fig. 1 Influence of the density on rolling contact fatigue [3]

Many published papers are dealing with roller tests of sintered specimens. Investigation with different alloys, different sintering temperatures and with different core densities as well as with surface densified specimens were carried out [2–12]. The results show a stringent relation between the density and the rolling contact fatigue, Fig. 1.

The influence of sintering temperature and alloying elements is marginal compared to the dependence on the density. Based on the results of roller tests, flank and root carrying capacity of different gear geometries were tested, [13–15]. These investigations show that PM gears are competitive to conventional gears.

3 Stress distribution in gears

As shown in Fig. 2, the highest stresses in a loaded gear tooth are located in the near surface region from where the stress level drops steadily with the distance from surface.

Introducing a high density, a high strength surface layer around the gear tooth should therefore increase the load carrying capacity of the gear. Reducing the surface porosity will reduce the notch effect that pores normally have, which also contributes to the improved performance of surface densified gears.

4 Process chain of surface densification

The process chain of PM parts starts with the powder production. For high density and high strength applications an iron molybdenum alloy is water atomized. Other alloying elements, usually copper and nickel, are diffusion bonded. The carbon is alloyed by powder mixing [16]. A fill shoe fills the powder in a cavity formed by the lower punches and the die. To obtain a homogenous density in complex and multilevel parts hydraulic presses are used. The advantage of hydraulically controlled presses is the separate control of every single punch. The cracking is prevented by the fact that all punches reach the pressing

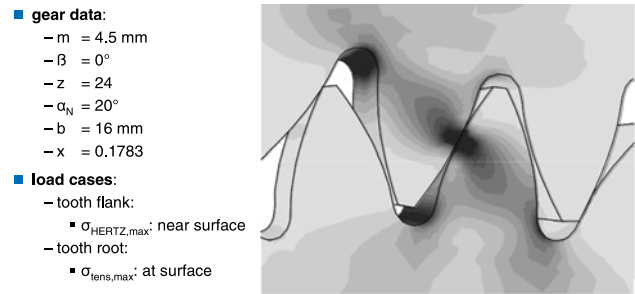


Fig. 2 Finite element tension analysis of rolling gears

positions simultaneously and that a force reduction is attached after the pressing cycle. To attain sufficient mechanical properties by diffusion bonding, the green parts are sintered at conventional sintering temperature of $\theta_{sinter, conv} = 1,120^\circ \text{C}$ or in modern furnaces at temperatures up to $\theta_{sinter, high} = 1,290^\circ \text{C}$. High temperature sintering improves the diffusion rate, so that better mechanical properties can be achieved. Additionally the range all logging elements, e.g. chromium, can be expanded by using higher temperatures during sintering. The surface densification operation is placed after the sintering process. Two basically different processes are in use for the surface densification, translatory methods [17, 18], and rotatory methods [19–22]. The more common method is the rolling process, where the sintered gear is mounted between two master gears, shown in Fig. 3.

The required pressure to deform the material is generated by a radial force.

Surface densified gears have to meet mainly three requirements.

- A sufficient depth of the densified layer is required to reach the postulated strength.
- The gear has to meet the specified geometrical accuracy.
- The densification of the surface layer needs to be homogeneous.

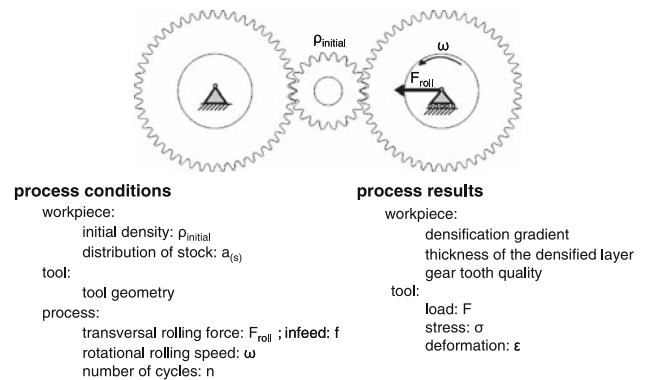


Fig. 3 Surface densification by rolling

Due to the theory of Hertz [23], the maximum effective stresses are found underneath the surface at a surface distance defined by the load, the geometry and the material properties. The densification depth and the density gradient define the material properties and have to take allowance for the distribution of the effective stresses.

Besides the strength, the geometrical accuracy of the gears is the most important component property. Usually for transmission gears of passenger cars a geometrical accuracy of DIN 3962Q7 is required by the automotive industry. Furthermore, the costs of the hard finishing operation depend directly on the amount of stock. In order to reduce the costs of hard finishing a dimensional accuracy of the PM gears after heat treatment near DIN 3962Q7 is required.

Distortions of PM parts caused by heat treatment depend on the local density. In order to achieve systematic and predictable distortion on hardening, the densified layer must have a continuous thickness. Furthermore the distortions can be estimated if the densification gradient is known.

Due to the porosity and especially due to the connectivity between the pores, heat treatment of PM parts differs from the heat treatment of wrought materials. The high reactivity with the atmosphere due to the large specific surface of porous materials, penetration of the porosity with quenching medium and reduced thermal conductivity of PM materials are the reason for special heat treatment routines. Low pressure carburizing with gas quenching or plasma carburizing are the most suitable heat treatment methods for PM parts [24, 25]. Due to the distortions after heat treatment, the gears have to be hard finished in many cases.

5 Need for FEA

Experiences with the rolling process after sintering have shown that the elastic-plastic behavior of PM materials and the continuous change of the contact conditions during rolling result in total profile and flank deviations as well as in partially incomplete densified regions. Due to the superposition of the constitutive behavior of PM materials and the complex kinematics of rolling gears, the rolling process is difficult to be described analytically. Moreover no previously published experiences exist to support the process design. Therefore, the process design is currently optimized by an iterative and cost intensive development. For a better understanding of the process, the numerical simulation is a suitable method [26–28]. Before experimental studies are carried out, the layout of a surface densification process can be simulated by means of FEA. Based on this, an optimized densification layer adjusted to

the load distribution can be dimensioned. Also the process parameters such as infeed and stock for rolling can be calculated using FEA. These calculated process parameters can be assigned to the subsequent surface densification rolling process.

Moreover, in forming of sintered parts, materials are more susceptible to fracture than in forming of solid materials. The analysis is therefore of particular importance in producing defect-free components by determining the effect of various parameters (density, rolling force, material, tool geometry, stock distribution and friction conditions) on the detailed metal flow.

6 Plasticity criteria for porous metals

In contrast to wrought materials the constancy of volume is not given for porous materials. Under a hydrostatic pressure contraction of the material is possible. This difference requires the implementation of a plasticity criteria which considers the change of volume. The key hypothesis of the theory of plasticity is usually based on the assumption of the existence of a plasticity criterion ϕ linking together the components of the stress tensor σ_{ij} . The deformation of a material is elastic when $\phi(\sigma_{ij}) < 0$, and becomes plastic when $\phi(\sigma_{ij}) = 0$.

In repressing type deformations, for example surface densification of compacted and sintered gears, pores collapse and align in the direction perpendicular to the direction of forging and result in local anisotropy. In characterizing the mechanical response of porous materials, a phenomenological approach (introducing a homogeneous continuum model) is employed. In contrast to the theory of plasticity of full dense materials the equations for sintered materials are coupled by means of porosity functions. The retention of volume is not given, if the hydrostatic stress component exceeds the yield stress, porous materials deform volumetrically and the density increases.

For isotropic, compressible material the plasticity potential $\phi(\sigma_{ij})$ is defined according to Kuhn and Downey [29], as a function of the invariants, ν_{pl} , the Poisson's ratio under plastic deformation, and Y_ρ , the yield stress of the porous material in uniaxial extension depending on the density:

$$\phi(\sigma_{ij}) = 3 \cdot I_2' - (1 - 2\nu_{pl})I_2 - Y_\rho^2 = 0 \quad (2)$$

In elastically deforming materials the Poisson's ratio is constant during deformation and is a property of the material. In plastic deformations of isotropic materials this ratio is one half due to the incompressibility of the material. This rule is not valid for porous materials, such that the plastic Poisson's ratio must be determined experimentally.

Kuhn and Downey have done the determination by doing compression test for a sponge iron sintered at a temperature of $\theta_{sinter} = 1,093^\circ \text{C}$. Using a least square method, the following power law was fitted to the experimental data.

$$v_{pl} = 0.5\rho_{rel}^{1.92} \quad (3)$$

A variation of the sintering temperatures has shown that the above named equation is valid for sintering temperature higher than the $\alpha \rightarrow \gamma$ transformation temperature.

I_1 and I_2 are the first (linear) and second (parallel) Invariants of the principal stress tensor and defined as, [30]:

$$I_1 = \sigma_x + \sigma_y + \sigma_z \quad (4)$$

$$I_2 = \sigma_x\sigma_y + \sigma_y\sigma_z + \sigma_x\sigma_z - \tau_x\tau_y - \tau_y\tau_z - \tau_x\tau_z \quad (5)$$

Since the parallel invariant of the principle stress tensor I_2 can be expressed by a function of the linear invariant of the principle stress tensor I_1 and the parallel invariant of the stress deviator I'_2 ,

$$I'_2 = \frac{1}{6} \left[(\sigma_x - \sigma_y)^2 + (\sigma_y - \sigma_z)^2 + (\sigma_z - \sigma_x)^2 \right] + (\tau_{xy}^2 + \tau_{yz}^2 + \tau_{zx}^2), \quad (6)$$

in the term:

$$I_2 = I'_2 - \frac{1}{3}I_1^2 \quad (7)$$

the plasticity criterion can be transformed to

$$\phi(\sigma_{ij}) = 3 \cdot I'_2 - \frac{1 - 2v_{pl}}{2(1 + v_{pl})} I_1^2 - \frac{3Y_\rho^2}{2(1 + v_{pl})} = 0 \quad (8)$$

The apparent yield stress Y_ρ of porous material depends on the property of the base material and the relative density ρ_{rel} . It has to match two conditions. First is that $Y_\rho = Y_b$ for the full dense state. Second is that for a density near the apparent density $Y_\rho = 0$. The apparent yield stress can be expressed by:

$$Y_\rho^2 = \eta \cdot Y_b^2 \quad (9)$$

where Y_b is the yield stress of the base material in the pore-free state and η is a function of relative density. The effects of strain, strain-rate, and temperature on yield stress are included in $Y_b = Y_b(\bar{\epsilon}_b, \dot{\bar{\epsilon}}_b, T_b)$, where $\bar{\epsilon}_b$, $\dot{\bar{\epsilon}}_b$ and T_b are strain, strain-rate and temperature of the base material.

To complete the constitutive equations, η must be determined as function of relative density by experiment, e.g. uniaxial compression tests. Among the proposed constitutive equations those suggested by Doraivelu et al. [31],

and by Shima et al. [32], appear to agree with experimental measurements quite well. Doraivelu has determined the expression for η by uniaxial compression tests at a testing temperature of $\theta_{test} = 400^\circ \text{C}$ for the aluminum alloy X7091 with initial densities of $\rho_{rel, initial} = 0.75$ and $\rho_{rel, initial} = 0.82$ and sintered at $\theta_{sinter, high} = 593^\circ \text{C}$. According to these investigations η can be described by:

$$\eta = 2\rho_{rel}^2 - 1. \quad (10)$$

Even though this equation was derived from experiments with aluminum powders, the relationship between η and ρ_{rel} can be used for iron powders as well. The adaptability of this equation for the powder used in this investigations was verified by modeling uniaxial compression test. The correlation between experimental and numerical results was excellent.

For the investigation in this paper the used material was water atomized, diffusion bonded Fe-Ni-Cu-Mo-C-alloy. The determination of the plastic behavior of the used material was carried out by means of compression tests on cylindrical specimens with diameter $d = 6 \text{ mm}$ and height $h = 10 \text{ mm}$. The parameters of the stress and plastic strain equation

$$k_f = A \cdot (B + \varphi)^C, \quad \varphi = \ln\left(\frac{1}{1 - \epsilon}\right), \quad (11)$$

were fitted judged on the basis of the sum of the squared residuals (SSR) to the values of

$$A = 1,341 \text{ N/mm}^2, \quad B = 0.0096, \quad C = 0.186.$$

To describe the elastic behavior, Young's Modulus and Poisson's ratio were calculated with an initial density of $\rho_{rel, initial} = 0.88$ by the equations according to Beiss to the values of:

$$E_{0.88} = 133,174 \text{ N/mm}^2 \text{ and } \nu_{el,0.88} = 0.262$$

For the finite element formulations of the equilibrium and energy based on the infinitesimal theory, the following assumptions are made: the elastic portion of deformation is neglected, the normality of the plastic strain rates to the yield surface persists, anisotropy that occurs during deformation is negligible, and thermal properties of the porous material are independent of the temperature.

7 FEA modeling

The conditions of the simulated surface densification process were taken from a previous experimental work. The

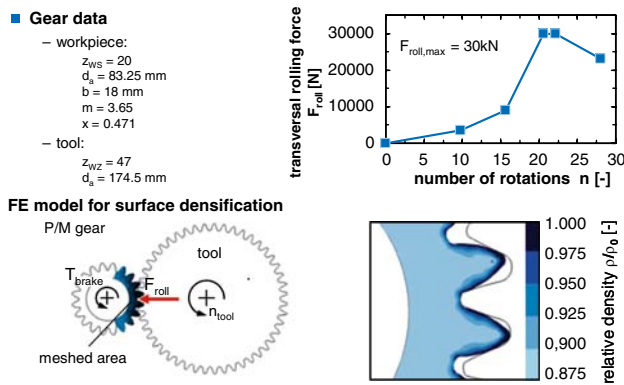


Fig. 4 Gear data and FEA model

PM gears were rolled on a transversal roll machine with a constant rotational speed. The flexible rolling process was force controlled with a maximum transversal force of $F_{roll,max} = 30$ kN. Gear data and transversal rolling force are shown in Fig. 4.

Aim of the FEA model development was to achieve a high flexibility of the model. The influence of varying process parameters on the process results could possibly be investigated by means of parameter variation. Due to the geometry of spur gears, a simulation in 2.5D model is an approximation close to the reality. The face width of the 2.5D model is assumed to $b_{2.5D} = 1$ mm, so that the transversal rolling force must be converted related to $b_{2.5D} = 1$ mm face width. Due to the symmetry, it is adequate to model just one of the tools. The introduced FEA model affords the variation of input data such as process parameters, geometry and material properties. Additionally simulation parameters and material parameters can be modified to verify the FEA model. The verification of the FEA model was done by the surface densification of rollers, which is not documented in this paper [33]. The criterion for the verification was the density distribution depending on the surface distance. The used FEA models are shown in Fig. 4.

The FEA model enables the flexible modeling of various processes under different process conditions. The boundary conditions of the model are composed of variable process parameters such as the transversal rolling force $F_{roll}(t)$, relative density ρ_{rel} , braking torque T_{brake} , the number of rolling cycles n and the material data of the workpiece $E(\rho)$, $\nu(\rho)$, $k_f(\rho, \theta, \epsilon)$. By adjusting the FE analysis parameters, the accordance of the model with reality can be optimized. These parameters are predefined by the element type of the mesh, the aforementioned boundary conditions as well as the analytical and empirical models of the plasticity theory as proposed by Gurson [34], Kuhn [29], Ponte Castañeda [35], Shima et al. [32], and Gologanu

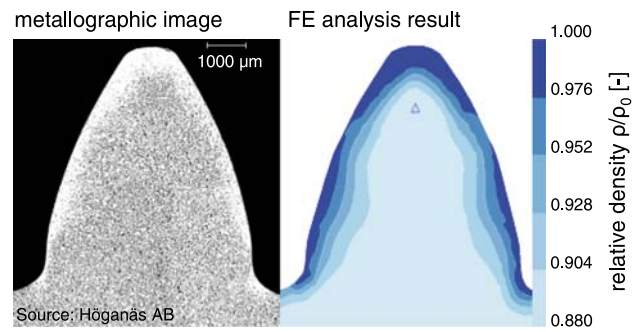


Fig. 5 Comparison of relative density

et al. [36]. The FE analysis results comprise density gradient ρ (a), gear quality and tool load F , σ_v and ϵ .

8 FEA results

The above named experimental investigation was simulated with the postulated FEA model using the commercial software tool SFTC-DEFORMTM. To compare the density distribution determined by the numerical simulation with the real density distribution metallographic specimens were prepared. The comparison of the density gradient determined by numerical simulation and experimental investigation is shown in Fig. 5.

Obviously the simulated result is in an excellent accordance with the reality. The tip of the tooth is quite strongly densified in both cases. The area of high density begins from the tip of the tooth and continues down the flank. Near the pitch diameter a low density area is found. The tooth roots are incompletely densified as well. Such as shown in the metallographic image, the numerical simulation shows a smaller high densified area in the left tooth root than in the right one.

The geometry of the tool is the reason for the insufficiently densified area on the flanks near the pitch diameter and in the tooth root. At the moment when the tool is in contact with the flank, the tool is supported by the tip of the tooth. The stress necessary for densification takes effect in the tooth tip and neither at the flank nor at the tooth root, Fig. 6.

This effect results in an intense densification at the tip and an insufficient densification in the functional areas.

The value of average maximum strain rate is calculated to $\dot{\epsilon}_{max,av} = 5.71$ s⁻¹ and the highest maximum strain rates occurring during the process are in the level of $\dot{\epsilon}_{max,max} = 25$ s⁻¹. The analysis of the strain rates shows that the maximum strain rates are found in two significant regions, Fig. 6.

In the area of the transition from tooth root to the involute high strain rates occur, when the tip of the tool

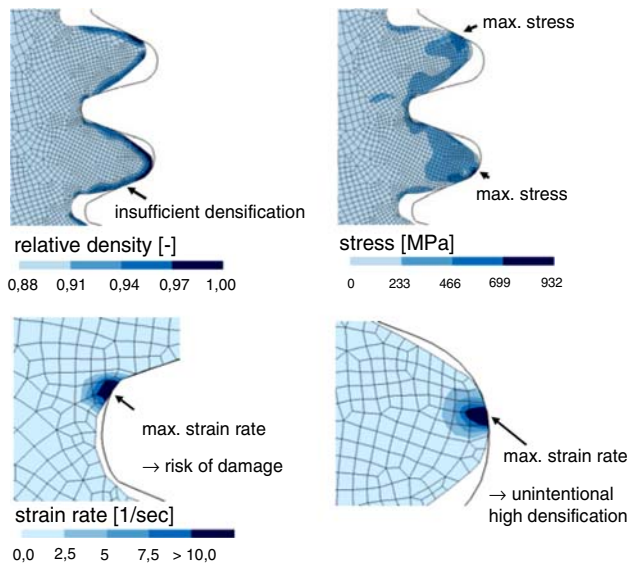


Fig. 6 Reason for insufficient densified areas and maximum strain rate during surface densification by rolling

scraps through the fillet due to the high relative velocities between tool and workpiece. Due to the high strain rates in this area scattering of the surface can occur in the tooth root. The second case for high strain rates is when the tooth root of the tool is supported only by the tip of the workpiece tooth. The whole transversal force is concentrated in a quite small area, resulting in high local stresses. A very high densification of the tip of the tooth is not intended, but due to the extremely high stresses the tip of the tooth is deeply densified in this case.

To find out more about the interrelationship between the process parameters and the achieved densification, parameter variations were carried out. Starting from the real process conditions with the above named initial density and transversal force a parameter matrix for the FE analysis was designed, with a fixed number of revolutions and varying transversal forces and densities. As criterion for comparison

the thickness of the densified layer $t_{D,98\%}$ was defined in the style of the case-hardening thickness and signifies the distance from the surface where 98% of the full density is obtained. The thickness of the densified layer was analyzed in the functional areas, perpendicular to the pitch diameter and perpendicular to the 30°-tangent at the tooth root. Figure 7 shows the results for the variation of the initial density and the variation of the transversal rolling force.

As expected, the thickness of the densified layer on the flank increases with higher initial densities. However, this effect can not be observed in the tooth root. The thickness of the densified layer is almost independent on the initial density. The superposition of two countered effects is the explanation for this observation. Due to the dependency of the Young's modulus of density, the stiffness of the teeth increases with increasing initial density. Due to the higher stiffness, the support of the tool by the workpiece is higher; such that a lower amount of the transversal rolling force reaches the ground of the tooth space. Contrarily the higher initial density has higher potential to reach the level of 98% of full density.

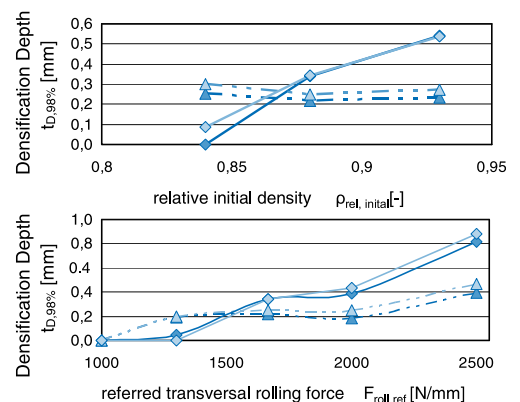
The variation of the transversal rolling force shows that rolling forces, referred to a face width of $b_{2.5D} = 1 \text{ mm}$, lower than $F_{roll,ref} = 1,000 \text{ N/mm}$ do not produce a full densified surface layer. Exceeding a transversal force of $F_{roll,ref} = 1,500 \text{ N/mm}$ the thickness of the densified layer increases with respect to the transversal rolling force. The curve progression, which describes a plateau in the area around $F_{roll,ref} = 1667 \text{ N/mm}$ describes the superposition of different effects in this case as well.

Finally the variation of the cycle number was carried out and the thickness of the densified layer analyzed, Fig. 8. The thickness of the densified layer increases progressively with the number of rolling cycles. The essential amount of densification is reached after three rolling cycles for common rolling forces. Low referred rolling forces below $F_{roll,ref} = 1,000 \text{ N/mm}$ are not sufficient to densify the surface layer to full density.

Fig. 7 Influence of the density and the rolling force on the thickness of the densified layer

- Variation of initial density
 - $F_{roll,ref} = 1667 \text{ N/mm}$
 - $n = 3$ in both rolling direction
- Variation of the transversal rolling force
 - $\rho_{rel} = 0.88$
 - $n_U = 3$ in both rolling directions

	tooth root	tooth flank
right	—▲—	—◆—
left	—▲—	—◆—



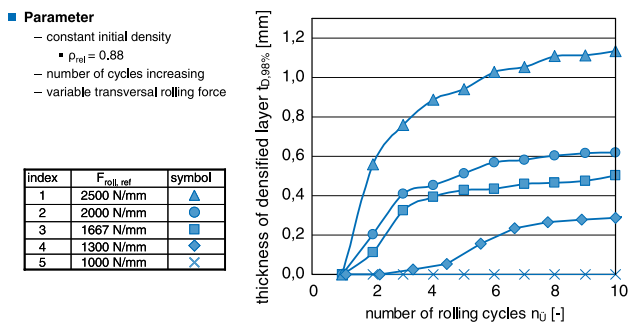


Fig. 8 Influence of the number of rolling cycles on the thickness of the densified layer

9 Conclusion

The surface densification process by rolling, experimentally investigated in a prior project, was modeled in a 2.5 DFEA model. For the model verification densifications of the tooth determined through simulations and through metallographic investigation were compared. An excellent agreement between the theoretical and experimental results was found. As shown in the metallographic investigation, the densification of the available gear was suboptimal in some areas. Via detailed analysis of the contact conditions between the tool gear and the workpiece gears during rolling the disadvantages of the process were identified. These results show that the FE analysis can broaden the process understanding and has the potential to be an effective tool for the process design and optimization.

Using the verified model parameter variations were carried out to increase the process knowledge. The thickness of the densified layer was evaluated for varying densities, rolling forces and numbers of rolling cycles. The results show that the density depending stiffness of the teeth and the tooth flanks has a significant influence on the densification. Due to the varying stiffness at different core densities the contact conditions between the tool and the workpiece are variable. Furthermore it was shown that at an advanced densified state saturation of the densification appears due to the strengthening of the material.

References

1. Beiss P (2003) Iron and steel: manufacturing route, chap 5, structural mass production. In: Landolt-Börnstein—Group VIII Advanced Materials and Technologies, pp 5–20
2. Hanejko F, Rawlings A, Narasimhan KSV (2005) Surface densified P/M steel—comparison with wrought steel grades. Euro PM2005, Prague, pp 509–511
3. Petersen J (2004) Wälzfestigkeitsuntersuchung von Sinterstählen und Neuentwicklung eines Wälzfestigkeitsprüfstands. Dissertation RWTH, Aachen University

4. Kotthoff G (2003) Neue Verfahren zur Tragfähigkeitssteigerung von gesinterten Zahnradern. Dissertation RWTH, Aachen University
5. Nigarura S, Trasorras JRL (2001) Rolling contact fatigue properties of DensiFormed™ sintered alloys advances in powder metallurgy and particulate materials. MPIF/APMI, Princeton, pp 155–168
6. Lipp K, Sonsino CM (2000) Hochfeste Sinterstähle—Einsatz hochfester umweltfreundlicher Sinterstähle für hochbelastbare Bauteile. Forschungskuratorium für Maschinenbau (FKM), Frankfurt/Main
7. Nigarura S, Blanchard P, Trasorras JRL (2001) Processing effects on rolling contact fatigue properties of sintered and DensiForme™ ferrous alloy. MPIF/APMI, Princeton, pp 16–35
8. Lawcock R, Buckley-Golder K, Sarafinchan D (1999) Testing of high endurance PM steels, for automotive transmission gearing components. In: Society of Automotive Engineers Paper 1999-01-0293
9. Jones PK, Buckley-Golder K, Lawcock R, Shivanath R (1997) Densification strategies for high endurance P/M components. Int J Powder Metallurgy 33(3):37–44
10. Strehl R (1997) Tragfähigkeit von Zahnradern aus hochfesten Sinterstählen. Dissertation RWTH, Aachen University
11. Chidester AJ, Green WB, Corbo K (1993) High-Hardness, High-Density Powder Metal Bearing Applications. ASTM, Philadelphia
12. Cadle TM, Landgraf CJ, Brewin P, Nurthen P (1991) Rolling contact of P/M steel—effects of sintering temperature and material density advances in powder metallurgy and particulate materials. MPIF/APMI, Princeton, pp 175–182
13. Trasorras JRL, Nigarura S, Sigl LS (2006) DensiForm® technology for wrought-steel-like performance of powder metal components. In: Society of Automotive Engineers Paper 2006-01-0398
14. Forden L, Bengtsson S, Bergström M (2005) Comparison of high performance PM gears manufactured by conventional and warm compaction and surface densification. Powder Metallurgy 48(1):10–12
15. Sandner C, Ratzl R, Lorenz B, Tobie T (2002) Sintered gears—achievable load-carrying capacities by conventional and new production methods. In: International conference on gears, Munich, pp 295–310
16. Höganäs AB (1998) Eisen- und Stahlpulver für Sinterformteile. Firmenschrift der Höganäs AB, Höganäs
17. Trasorras JRL, Riley ET (2006) US007025929B2: Method and apparatus for densifying powder metal gears
18. Woolf RM (2005) US006899846B2: Method of producing surface densified metal articles
19. Woolf R (2003) US006517772B1: Apparatus and method for forming powder metal gears
20. Woolf RM, Trasorras JRL (2000) US006151941A: Apparatus and method for roll forming gears
21. Shivanath R, Peter J (1998) US005729822A: Gear
22. Cole CJ, Shivanath R, Jones P (1998) US005711187A: Gear wheels rolled from powder metal blanks and method of manufacture
23. Hertz H (1895) Über die Berührung elastischer Körper, Leipzig
24. Altena H, Danninger H (2005) Wärmebehandlung von Sinterstahl-Präzisionsteilen, Part 2: Prozess und Anlagentechnik. BHM Berg- und Hüttenmännische Monatshefte 150(5):170–175
25. Danninger H, Altena H (2005) Wärmebehandlung von Sinterstahl-Präzisionsteilen, Part 1: Basic considerations. BHM Berg- und Hüttenmännische Monatshefte 150(3):77–81
26. Bassan D, Asit A, Pidria MF, Zingale P (2005) PM surface densification technology: a numerical-experimental methodology for rolling tool design. Euro PM2005, Prague, pp 217–224

27. Bassan D (2004) Asti M, Pidria M, Zingale, P.: A new simulation methodology for PM surface densification process. Euro PM2004, Vienna
28. Engström A (2003) FEM simulations of gear surface densification. Mini Thesis, Swedish Institute for Metals Research
29. Kuhn HA, Downey CL (1971) Deformation characteristics and plasticity theory of sintered powder materials. *Int J Powder Metallurgy* 7(1):15–25
30. Weichert D (1999) *Mechanik II für Ingenieure : Festigkeitslehre*. RWTH, Aachen University, Aachen
31. Doraivelu SM, Gegel HL, Gunasekera JS, Malas JC, Morgan JT (1984) A new yield function for compressible P/M materials. *Int J Mech Sci* 26:527
32. Shima S, Oyane M (1976) Plasticity theory for porous materials. *Int J Mech Sci* 18:285
33. Kauffmann P (2005) *Numerische Simulation des Oberflächenverdichtens von gesinterten Zahnrädern durch Querwalzen*. Mini Thesis, Laboratory of Machine Tools and Production Engineering, RWTH, Aachen University
34. Gurson AL (1975) *Plastic flow and fracture behavior of ductile materials incorporating void nucleation, growth and interaction*. Dissertation, Brown University
35. Ponte Castañeda P, Zaidman M (1994) Constitutive models for porous materials with evolving microstructure. *J Mech Phys Solids* 42:1459–1497
36. Gologanu M, Leblond JB (1993) Approximate models for ductile metals containing non-spherical voids - case of axisymmetric prolate ellipsoidal cavities. *J Mech Phys Solids* 41:1723–1754